Resonant-Raman-scattering study of disorder effects in $Al_xGa_{1-x}As$ alloys

M. E. Delaney,* T. C. McGlinn,† and M. V. Klein
Department of Physics and Materials Research Laboratory, University of Illinois, 1110 West Green St., Urbana, Illinois 61801

H. Morkoç
Coordinated Science Laboratory, University of Illinois, 1101 West Springfield Ave., Urbana, Illinois 61801

(Received 25 March 1991)

We use resonant Raman scattering to investigate the frequency difference between the longitudinal-optical phonon modes seen in dipole-forbidden and dipole-allowed polarization geometries in $Al_xGa_{1-x}As$ alloys. This splitting is studied as a function of laser photon energy, aluminum mole fraction x, and the indirect versus direct nature of the electronic band gap. Resonant Raman scattering, through the electron-phonon interaction, is a sensitive microscopic probe of the effects of short-range alloy disorder. For x in the indirect-gap regime, the dominant intermediate resonant state is a Γ-valley hole plus an X-valley electron that becomes effectively localized because of its short inelastic lifetime. Raman scattering via this state is described by a calculation of the Raman susceptibility that considers the random-alloy potential generated by local concentration fluctuations.

I. INTRODUCTION

$Al_xGa_{1-x}As$ alloys are the most studied of semiconductor alloys because of their usefulness in heterostructures with GaAs, to which they are closely lattice matched. For small x the material has a direct energy gap which increases with x and becomes indirect for x near 0.4. Resonant Raman scattering (RRS) is a sensitive probe of the direct band gap and related properties. It examines the electron-phonon interaction and effects of alloy disorder as the conduction-band minimum, dependent on the Al concentration x, changes from the zone-center Γ point to the zone-edge X point.

Tsu, Kawamura, and Esaki[1] performed the first detailed Raman study of $Al_xGa_{1-x}Ga$. They identified the two-mode behavior of the longitudinal-optic (LO) phonon over the entire range of composition, a result confirmed by Kim and Spitzer.[2] Jusserand and Sapriel studied the concentration-dependent asymmetric broadening of LO modes.[3] To explain their results, they applied a spatial correlation model, refined by Parayanthal and Pollack,[4] with correlation length scales of 100 Å. This model has since been challenged by Kash *et al.*,[5] who have shown through nonequilibrium anti-Stokes Raman scattering that the alloy phonons are essentially nonlocalized bulk-like modes, at least on the 0–1000-Å scale.

Regarding resonance Raman scattering, Shah *et al.*[6] performed an unpolarized RRS study and observed a strong resonance for the first- and second-order scattering of the LO modes when the outgoing photon energy equaled that of the resonant electronic state, which they identified as a intermediate exciton associated with the direct gap. In agreement with studies of indirect GaP, they found no resonance feature to associate with the indirect gap.

We have studied $Al_xGa_{1-x}As$ alloys grown by molecular-beam epitaxy (MBE) via RRS. Figures 1 and 2 show the Raman spectra for the "GaAs-like" (denoted by subscript 1) and "AlAs-like" (denoted by subscript 2) LO modes under resonant excitation with laser photon energies close to the direct (E_0) band gap. The unexpected feature of these spectra is the small but definite shift in peak position of the phonon line between the spectrum taken in the dipole-allowed polarization geometry wherein the electron-phonon coupling occurs via deformation-potential scattering [$z(x,y)\bar{z}$ geometry (unprimed)] and the spectrum taken in the dipole-forbidden geometry wherein the coupling occurs via intraband Fröhlich scattering [$z(x,x)\bar{z}$ geometry (primed)]. Defining $\Delta\omega=\omega_0'(\text{forbidden})-\omega_0(\text{allowed})$, we find at 1.94 eV for the $Al_{0.41}Ga_{0.59}As$ sample that $\Delta\omega_1=1.0\ cm^{-1}$ for the GaAs-like mode (LO_1) and $\Delta\omega_2=-1.6\ cm^{-1}$ for the AlAs-like mode (LO_2). These shifts vary and change sign

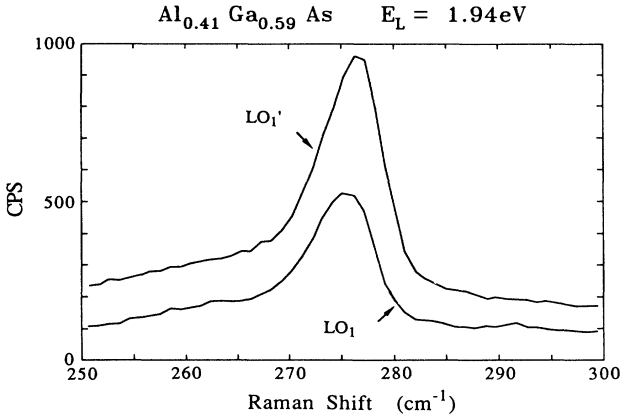

FIG. 1. GaAs-like dipole-allowed LO_1 and dipole-forbidden $LO_{1'}$ phonons for $Al_{0.41}Ga_{0.59}As$ with a resonant laser energy below the direct gap. Note the $LO_{1'}$ is shifted to higher energy.

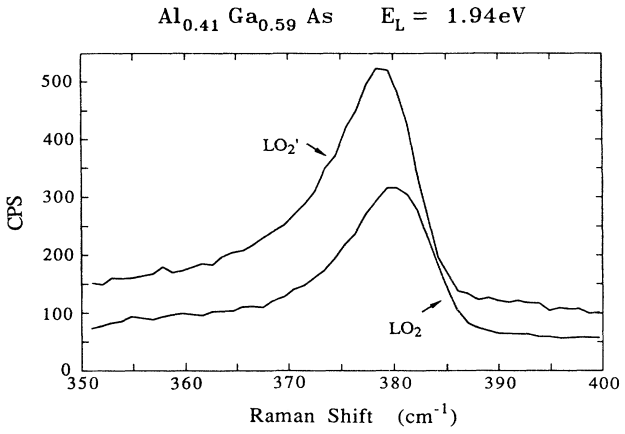

FIG. 2. AlAs-like dipole-allowed LO_2 and dipole-forbidden $LO_{2'}$ phonons for $Al_{0.41}Ga_{0.59}As$ with a resonant laser energy below the direct gap. Note that $LO_{2'}$ is shifted to lower energy.

as the laser photon energy is tuned through the direct-gap resonance. The presence and strength of this effect depends upon whether the fundamental gap is direct, near crossover, or indirect. Beserman *et al.*[7] and McGlinn, Klein, and Morkoç[8] where the first to observe this shift. Sela *et al.*[9] later analyzed it using the concept of local Al concentration fluctuations occurring in the effective electron-phonon interaction volume.

Resonant Raman scattering by LO phonons involves both a short-range (deformation potential) and long-range (intraband Fröhlich) component of the electron-phonon interaction. The deformation-potential and interband Fröhlich (also known as the electro-optic contribution) interactions are independent of phonon wave vector $\mathbf{q}$ and lead to the usual allowed $\mathbf{q}=0$ zone-center selection rules observed in $z(x,y)\bar{z}$ scattering geometry. The q-dependent Fröhlich interaction appears in the $z(x,x)\bar{z}$ geometry and has a Raman-scattering efficiency proportional to q^2. For an intrinsic first-order process, this essentially vanishes in the $\mathbf{q}=\mathbf{k}_L-\mathbf{k}_S\approx 0$ approximation of allowed scattering. Here $\mathbf{k}_{L,S}$ are the wave vectors of the laser and scattered photons. Martin[10] showed that nevertheless one obtains a strongly resonant intraband Fröhlich Raman efficiency that can be important in spite of the small value of q^2. Gogolin and Rashba[11] proposed an additional mechanism that in effect replaces the kinematic $\mathbf{q}=\mathbf{k}_L-\mathbf{k}_S$ by a larger quantity due to impurities. They considered a higher-order perturbation where the intermediate electron-hole pair scatters twice, once through an electron-impurity interaction gaining wave vector $\mathbf{q}$ from the impurities and once through an electron-phonon interaction yielding wave vector $\mathbf{q}$ to the LO phonon. Though of higher order in perturbation theory than the intrinsic mechanism, this term is free from the restriction to small phonon wave vectors, and it actually dominates over the intrinsic scattering in alloys, where the relaxation of wave-vector conservation results from alloy scattering. Generated by the random group-III element mixing, the scattering potential V may be defined as the local deviation from the average potential made in the virtual-crystal approximation. More precisely, V must be defined as the random potential remaining after configurational averages of one-electron propagators are taken, using, for example, the coherent-potential approximation. However defined, the effect of the random-alloy potential is designated in the literature as "extrinsic."

Section II describes the details of the Raman experimental apparatus and the $Al_xGa_{1-x}As$ samples. Section III discusses our measurements, specifically the role of the directness of the gap in Sec. III A, the resonance profiles in Sec. III B, and the slope of shifts in Sec. III C. We outline our model to explain the shift in Sec. IV with the motivation discussed in Sec. IV A. In Sec. IV B we calculate the Raman susceptibility to second order in the disorder potential. Section IV C treats a similar random-alloy potential calculation to first order, and Sec. IV D evaluates our results. We summarize in Sec. V.

II. EXPERIMENTAL METHODS

The $Al_xGa_{1-x}As$ alloys were grown by MBE on Si-doped (001) GaAs substrates. A 0.3–1.0-μm GaAs layer buffered the 1–2-μm-thick alloy layers. The higher-Al-concentration samples were capped by a final 200-Å GaAs layer to retard oxidation. The nominal concentrations were $x=0.26$, 0.41, 0.42, 0.45, 0.68, and 0.77 as determined through luminescence and Raman measurements. The $Al_{0.26}Ga_{0.74}As$ and $Al_{0.42}Ga_{0.58}As$ layers were grown at 620 °C, and the other samples were grown at 700 °C. Compositional uncertainty is not critical to our analysis, since the key features are that $Al_{0.26}Ga_{0.74}As$ is a direct-gap sample and $Al_{0.41}Ga_{0.59}As$ is an indirect-gap sample slightly past crossover.

The Raman spectra were recorded by a Spex model 1400 double monochromator with 1800-line/mm holographic gratings outfitted with a photomultiplier tube in photon-counting mode. Some of the resonance profiles were made using a Spex 1877A Triplemate monochromator/spectrograph accompanied by a Photometrics CCD camera system. The samples were mounted in a Janis Super Vari-temp liquid-helium cryostat in a pseudobackscattering configuration. Most of the measurements were made at room temperature. A polarization analyzer was placed at the entrance slit of the spectrometer to distinguish between scattered light polarized parallel ($[z(x,x)\bar{z}]$) or perpendicular ($[z(x,y)\bar{z}]$) to the polarization of the incident laser light. Ar^+ and Kr^+ cw ion lasers and an Ar^+-pumped Coherent model 490 dye laser with Rhodamine 590 or DCM served as light sources.

III. EXPERIMENTAL RESULTS

A. Directness of gap

We found no observable shifts in purely direct-gap samples, i.e., $\Delta\omega_1\simeq\Delta\omega_2\cong 0$. The Raman signal was swamped by luminescence for laser photon energies

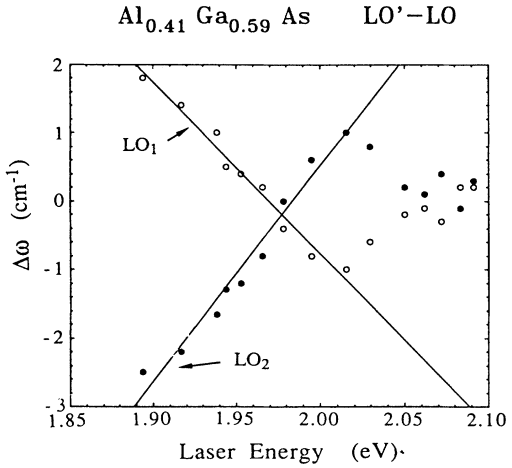

FIG. 3. $Al_{0.41}Ga_{0.59}As$ phonon frequency difference of the dipole-forbidden modes from their dipole-allowed counterparts as a function of laser energy.

below E_g^Γ for the $Al_{0.26}Ga_{0.74}As$ sample, but at a laser photon energy 20 meV above E_g^Γ there was no shift for LO_1 or LO_2. There is also no observable shift at the $E_0+\Delta_0$ resonance in $Al_{0.26}Ga_{0.74}As$. However, in an indirect alloy just past crossover, $Al_{0.41}Ga_{0.59}As$, the shifts persisted for laser energies E_L 70 meV above the direct gap at 1.98 eV, as shown in Fig. 3. Figure 4 shows that the effect persisted in the $Al_{0.42}Ga_{0.58}As$ alloy for laser photon energies 100 meV above $E_g^\Gamma=1.99$ eV. The $Al_{0.68}Ga_{0.32}As$ and $Al_{0.77}Ga_{0.23}As$ samples, much more indirect than the others, demonstrated a shift for $E_L > E_g^\Gamma$.

The reproducibility of the value of the energy of the scattered photon for the two polarizations was insufficient to clearly establish in a single run whether the nonzero value for the shift $\Delta\omega$ was due to a dependence of the photon frequency ω_0'(forbidden) or ω_0(allowed) on laser photon energy. Statistical analysis of the peak positions of many runs indicated that the ω_0' spectrum coupled via the Fröhlich interaction $[\bar{z}(x,x)z]$ is laser energy dependent. LO-mode frequencies vary with Al concentration x approximately linearly, the GaAs-like mode decreasing and the AlAs-like mode increasing versus increasing x. We note that the peak due to the Fröhlich interaction is higher (lower) in energy than that due to the deformation potential for the LO_1 (LO_2) mode for incident laser energy below the gap E_g^Γ. The opposite is true for laser energy above E_g^Γ. The observed behavior of $\Delta\omega$ versus laser photon energy is consistent with the notion that the Fröhlich-mediated scattering occurs predominantly in local GaAs-rich regions for $E_L < E_g^\Gamma$ and in AlAs-rich regions for $E_L > E_g^\Gamma$. This picture is supported by observations of Sela *et al.*[9] for the dipole-forbidden intensity ratio of LO_1 to LO_2. This ratio was found to be greater than unity below the direct gap, whereas above it was less than unity, a result we have confirmed.

B. Resonance profiles

Figure 5 displays the resonance profile for the $Al_{0.45}Ga_{0.55}As$ sample versus the resonance energy. The forbidden $z(x,x)\bar{z}$ profile, shifted by the 47 meV energy of the LO_2 phonon, shows an outgoing resonance at the gap energy 2.03 eV. The allowed $z(x,y)\bar{z}$ profile, shifted by 23.5 meV, shows an unresolved superposition of an incoming and outgoing resonance at 2.03 eV. Figure 6 shows similar profiles for the LO_1 mode of the same sample. The forbidden profile has been shifted 34 meV and the allowed by 17 meV. Finally, the $z(x,x)\bar{z}$ resonance profile is shown in Fig. 7 for the $Al_{0.41}Ga_{0.59}As$ sample

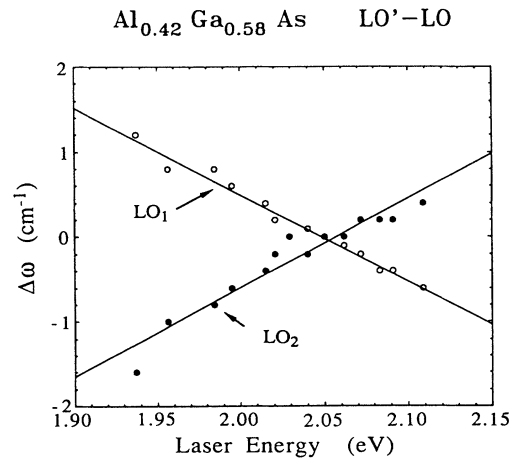

FIG. 4. $Al_{0.42}Ga_{0.58}As$ phonon frequency difference of the dipole-forbidden modes from their dipole-allowed counterparts as a function of laser energy.

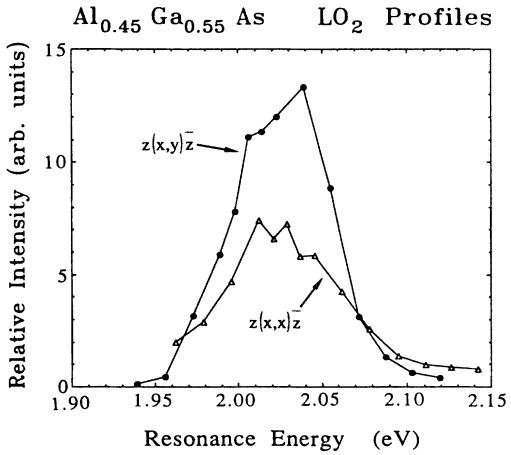

FIG. 5. AlAs-like resonance Raman profiles for the dipole-allowed $z(x,y)\bar{z}$ and dipole-forbidden $z(x,x)\bar{z}$ geometries. The forbidden profile is shifted -47 meV and the allowed is shifted -23.5 meV to reveal the resonant energy $E_g^\Gamma=2.03$ eV. Accuracy: intensity, $\pm15\%$; energy, ±0.5 meV.

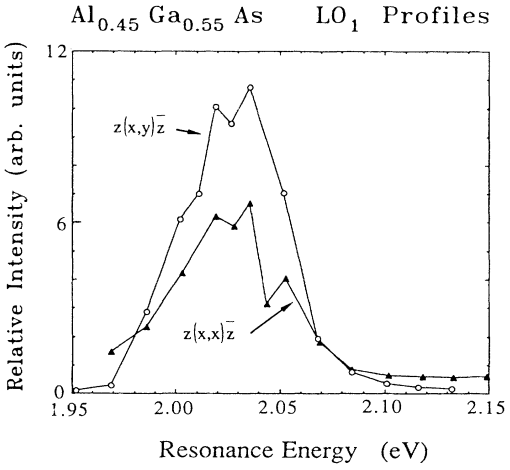

FIG. 6. GaAs-like resonance Raman profiles for the dipole-allowed $z(x,y)\bar{z}$ and dipole-forbidden $z(x,x)\bar{z}$ geometries. The forbidden profile is shifted -34 meV and the allowed is shifted -17 meV to reveal the resonant energy $E_g^{\Gamma}=2.03$ eV. Accuracy: intensity, $\pm 15\%$; energy, ± 0.5 meV.

for its LO_2 mode, LO_1 mode, and the second order difference mode LO_2-LO_1. Shifting each profile by its respective phonon energy identifies the direct energy gap at 1.995 eV.

The out resonance found for the $z(x,x)\bar{z}$ polarization is consistent with our expectation of an extrinsic forbidden intraband Fröhlich mechanism. In their study at the $E_0+\Delta_0$ gap of GaAs and (Cd,Hg)Te, Menendez, Cardona, and Vodopyanov[12] showed that first-order extrinsic scattering resonates at $E_L=E_g^{\Gamma}+\hbar\omega_0$, representing an outgoing resonance. Such behavior is expected from the scattering mechanism discussed earlier wherein the intermediate exciton scatters both through interaction with disorder and via phonon creation. The restriction to small phonon wave vectors is relaxed in this case. The intrinsic one-LO-phonon resonance peaks at $E_L=E_g^{\Gamma}+\hbar\omega_0/2$, halfway between an ingoing and outgoing resonance. The reason is because alloy and thermal broadening effects prevent resolution of the separate ingoing and outgoing peaks.

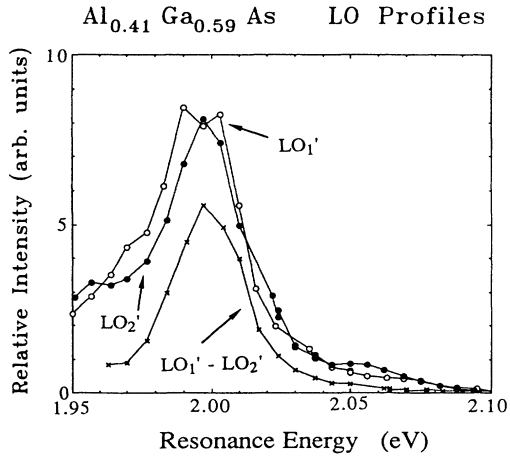

FIG. 7. Dipole-forbidden $z(x,x)\bar{z}$ GaAs-like, AlAs-like, and their difference-mode resonance Raman profiles for $Al_{0.41}Ga_{0.59}As$. Since these are outgoing resonance, each profile has been shifted down by its characteristic energy to reveal $E_g^{\Gamma}=1.995$ eV. Accuracy: intensity, $\pm 15\%$; energy, ± 0.5 meV.

TABLE I. Experimental widths of the resonance profiles for the LO_2 phonon (dipole-forbidden Fröhlich mechanism).

Sample	LO_2 FWHM	Temperature
$Al_{0.41}Ga_{0.59}As$	40 meV	300 K
$Al_{0.45}Ga_{0.55}As$	70 meV	300 K
$Al_{0.68}Ga_{0.32}As$	185 meV	10 K

The resonance profiles were found to broaden and weaken as the samples become more indirect. The full width at half maximum (FWHM) for the forbidden LO_2 mode is 40 meV for $Al_{0.41}Ga_{0.59}As$, 70 meV for $Al_{0.45}Ga_{0.55}As$, and 185 meV for $Al_{0.68}Ga_{0.32}As$, as listed in Table I. This broadening is comparable to that observed by Bosio *et al.*[13] in an optical transmission study of five samples from $Al_{0.36}Ga_{0.64}As$ to $Al_{0.61}Ga_{0.39}As$. They measured about a factor of 5 increase in linewidth.

A typical $z(x,x)\bar{z}$ Raman spectrum near resonance is shown in Fig. 8 for $Al_{0.41}Ga_{0.59}As$, a sample near crossover. In contrast to the direct-gap case where the luminescence is intense, the Raman signal is easily observed. If the laser photon energy remains in resonance near the direct gap, as the Al fraction x increases into the indirect-gap region, elastic-scattering channels are opened for electrons, first to the X valleys and then to the L valleys.

We next show in Fig. 9 the $E_0+\Delta_0$ resonance profile

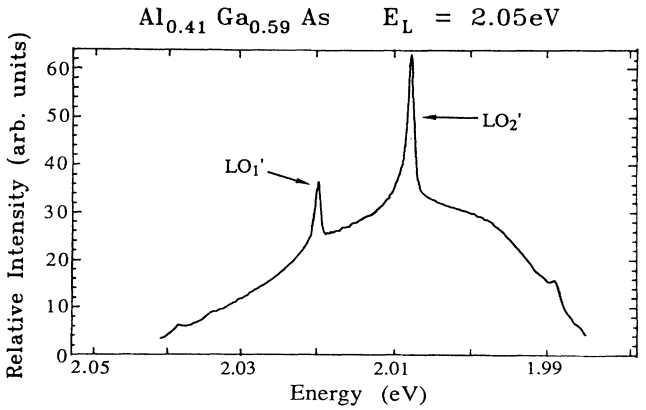

FIG. 8. $Al_{0.41}Ga_{0.59}As$ Raman spectrum illustrating the phonon modes atop a broad room-temperature luminescence, a signature of the outgoing resonance.

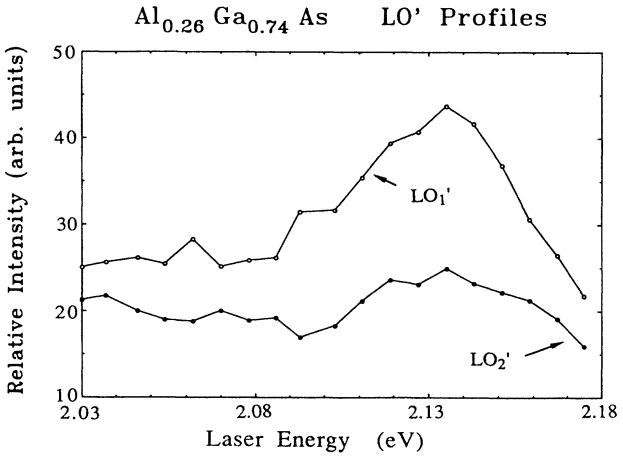

FIG. 9. $Al_{0.26}Ga_{0.74}As$ dipole-forbidden $z(x,x)\bar{z}$ $LO_{1'}$ and $LO_{2'}$ Raman profiles in resonance with the split-off gap. Accuracy: intensity, ±15%; energy, ±0.5 meV.

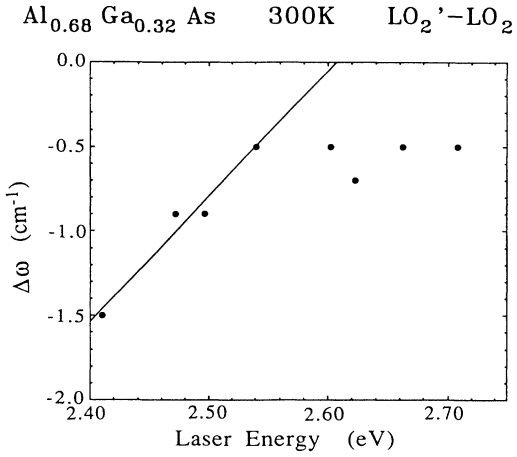

FIG. 10. $Al_{0.68}Ga_{0.32}As$ frequency shift between the dipole-forbidden $LO_{2'}$ mode and its dipole-allowed LO_2 counterpart vs laser energy at room temperature. These data show a constant -0.5-cm^{-1} shift at high energies away from the resonance peak at 2.40 eV or below.

for $Al_{0.26}Ga_{0.74}As$. Since this is a resonance with the spin-orbit gap, there is significant lifetime broadening and only weak luminescence.

C. Slope of shifts

The "shift slopes" $d\Delta\omega/dE_L \approx d\omega_{LO}(\text{Fröhlich})/dE_L$ of the shifts are tabulated in Table II. For LO_2 they decrease as the Al concentration increases. The LO_1 mode was too weak to track in the $Al_{0.68}Ga_{0.32}As$ and $Al_{0.77}Ga_{0.23}As$ samples. Figures 3 and 4 show the shift $\Delta\omega$ as a function of laser energy for the $Al_{0.41}Ga_{0.59}As$ and $Al_{0.42}Ga_{0.58}As$ alloys. The slopes of the straight-line portions of the curves differ sharply, with a change from 32 to 10 cm^{-1}/eV for the LO_2 mode. We observe a similar drop in the LO_1 mode from -25 cm^{-1}/eV, for $Al_{0.41}Ga_{0.59}As$ to -10 cm^{-1}/eV for $Al_{0.42}Ga_{0.58}As$. We did not pursue a detailed measurement of the $Al_{0.45}Ga_{0.55}As$ slopes other than to establish their presence. The high-resolution Raman work was best performed on the scanning spectrometer, whereas the multichannel system produced most of the resonance profiles.

In the more indirect samples, the shift slopes of the LO_2 modes are 7 and 8 cm^{-1}/eV for $Al_{0.77}Ga_{0.23}As$ and $Al_{0.68}Ga_{0.32}As$, respectively. Figure 10 shows the shift versus energy for $Al_{0.68}Ga_{0.32}As$. We repeated our measurements for $Al_{0.68}Ga_{0.32}As$ at 4 K to better tune the resonance to the Ar^+-laser lines, and the profile is shown in Fig. 11. The shift for $Al_{0.68}Ga_{0.32}As$ at 4 K also levels off at about -0.5 cm^{-1}, and these data are shown in Fig. 12.

A simple picture for the variation of the phonon frequency $\omega_0'(\text{Fröhlich})$ with E_L starts with the assumption that local fluctuations in the alloy Al mole fraction x produce local LO-phonon energy values $\omega_0(x)$ and local band-gap values. At the outgoing resonance, light is emitted from regions having local gap values obeying $E_g^{\Gamma}(x)=E_L-\hbar\omega_0(x)$. Within this picture the laser tracks the direct gap, and we may approximate the slope

TABLE II. Experimental shift slopes in cm^{-1}/eV.

Sample	LO_1	LO_2	Temperature
$Al_{0.41}Ga_{0.59}As$	−25.1	31.6	300 K
$Al_{0.42}Ga_{0.58}As$	−10.2	10.5	300 K
$Al_{0.68}Ga_{0.32}As$		7.4	300 K
		8.1	10 K
$Al_{0.77}Ga_{0.23}As$		6.4	300 K
		6.8	10 K

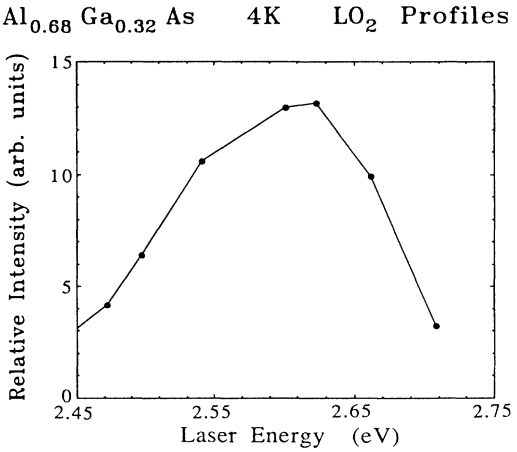

FIG. 11. $Al_{0.68}Ga_{0.32}As$ $LO_{2'}$ resonance Raman profile at 4 K. The gap has been temperature "tuned" to the energies of the Ar^+ laser. Accuracy: intensity, ±15%; energy, ±0.5 meV.

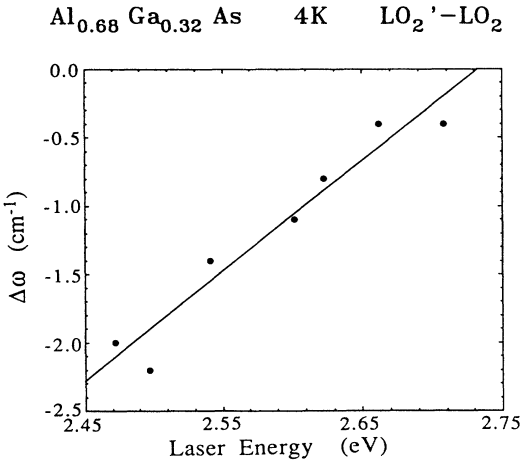

FIG. 12. Associated $LO_{2'}$ shift for the $Al_{0.68}Ga_{0.32}As$ resonance profile shown in Fig. 11. Again, we observe only negative values for this highly indirect sample.

$d\omega_0/dE_L$ as just $d\omega_0/dx$ divided by dE_g^Γ/dx. This argument generates the two solid curves in Fig. 13. We have used Adachi's[14] expression for the x dependence of the phonon frequency and the work of Lee, Juravel, and Wooley[15] for the x dependence of the alloy energy gaps. We chose the values of Lee, Juravel, and Woolley for a complete set of expressions for $E_g^\Gamma(x)$, $E_g^X(x)$, and $E_g^L(x)$. Table III shows the x dependence of the LO_1- and LO_2-phonon energies as well as the linearized expressions for the energy gaps near $x=0.5$ and 0.7.

This simple picture has several shortcomings. It yields slopes with magnitudes consistently higher than experiment, and the shift does not fade with increased Al content. The LO_2 shift in the two more indirect samples displayed only negative values. The $Al_{0.41}Ga_{0.59}As$ shifts crossed zero at the gap energy, the $Al_{0.42}Ga_{0.58}As$ shifts crossed zero 50 meV above, and the $Al_{0.68}Ga_{0.32}As$ shift never crossed zero. Most importantly, however, this picture does not explain the fact of no observable shift at the direct gap.

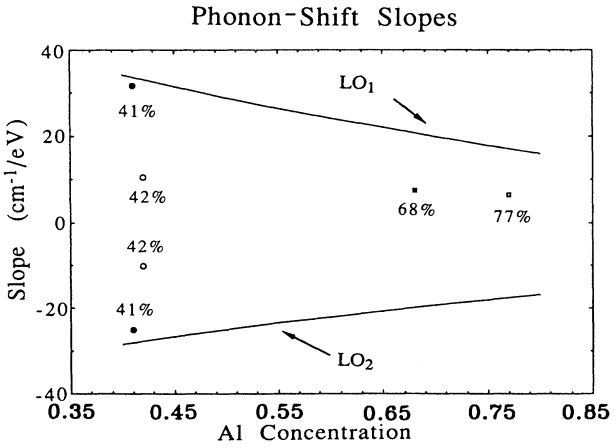

FIG. 13. Experimental phonon shift slopes compared to a simple model which assumes that the incident laser tracks the direct gap, that is, $d\omega_0/dE_L$ is $d\omega_0/dx$ divided by dE_g^Γ/dx.

TABLE III. Physical parameters for the model.

Physical parameters	
LO_1 (meV)	$36.25-6.55x+1.79x^2$
LO_2	$44.63+8.78x-3.32x^2$
E_g^Γ ($x_0=0.5$) (eV)	$1.333+1.525x$
E_g^X ($x_0=0.5$)	$1.850+0.250x$
E_g^Γ ($x_0=0.7$)	$1.244+1.673x$
E_g^X ($x_0=0.7$)	$1.794+0.343x$
γ'_{el} ($x_0=0.5$)	0.005
γ'_{in} ($x_0=0.5$)	0.075
γ'_{el} ($x_0=0.7$)	0.050
γ'_{in} ($x_0=0.7$)	0.200
m_Γ (m_0)	$0.067+0.083x$
m_{X1}	$0.257-0.067x$
m_{Xt}	$1.8-0.7x$

IV. MATHEMATICAL MODEL AND DISCUSSION

A. Introduction

We believe that a theory of "forbidden" resonance Raman scattering in alloys must use breakdown of wave-vector conservation due to alloy fluctuations (Gogolin and Rashba,[11] as discussed in the Introduction) as an essential ingredient. A formally correct theory of the observed coupling between the phonon energy seen via the Fröhlich mechanism and photon energy must also include (i) the effect of correlated scattering from the same fluctuation in alloy concentration of both the virtual electron-hole pair and phonon and (ii) propagation of the electron-hole system to include both elastic and inelastic scattering. Elastic scattering could lead to localization effects. Inelastic scattering could be real, due to phonon scattering, or, in the case of electrons in the Γ valley, "effective" due to alloy-induced elastic scattering of the electron to an indirect valley, X or L, where it would subsequently suffer a fast inelastic-scattering event, thus losing temporal coherence. To avoid extra complexity, we choose to neglect Coulomb (exciton) effects. We know of no correct method to include (i), in reality a complicated vertex effect, but we believe that a crude correction might suffice if inelastic scattering dominates under (ii). When the inelastic lifetime is shorter than the elastic lifetime, localization effects can be neglected, as self-energy and vertex corrections are dominated by simple inelastic lifetime broadening. Fluctuations in alloy concentration are decoupled if they are spatially separated by a distance of more than the inelastic mean free path, but within this distance there will be a coupling between the local value of the energy gap and phonon energy.

We use a model for the Raman susceptibility that ac-

counts for the role of fluctuations in alloy concentration x. This method utilizes a weighted averaging of the phonon frequency as developed by Sela *et al.*[9] who assigned a Gaussian distribution to the fluctuations in x. In that work the resonance profile was treated crudely as a sole ingoing resonance at the local energy gap. It incompletely explained the energy shift between the allowed and forbidden modes. We believe the resonant processes to be much more complex: The scattered photon is resonantly emitted after a phonon is created by an X-valley electron. Because of the short inelastic mean free path Λ of this electron, its band gap (and the energy of the phonon it emits) depends on the local value of x, averaged over a volume equal to Λ^3.

The laser-energy-dependent shift is seen only in alloys, and it is present only in indirect-gap samples. At first glance this indirect-gap restriction suggests a lifetime effect—the shortened effective inelastic lifetime, a consequence of indirect valley scattering channels—subjects the electron's reduced interaction volume to greater compositional fluctuations. But no experimental shift was found for resonance Raman scattering at the split-off direct gap, where the inelastic lifetime is also short. We believe that even a short inelastic lifetime is insufficient to produce a measureable shift at the direct gap. The small electron mass at the direct gap yields a relatively long inelastic mean free path, averaging out alloy fluctuations.

The averaging effect is diminished at the indirect gap, where the electrons are heavier and hence slower. We argue here that for indirect-gap alloys the fate of electrons excited by light in resonance with the direct gap is dominated by elastic (effectively inelastic) scattering into the indirect valleys. Luminescence work by Sturge, Cohen, and Logan[16] has shown for $Al_{0.46}Ga_{0.54}As$ that the rate for disorder scattering, evident from no-phonon transitions, dominates over the phonon-scattering rate, visible from phonon sidebands. The presence of no-phonon luminescence and absorption in indirect alloys demonstrates the strength of the random potential. Dingle, Logan, and Nelson[17] showed that the direct valley state can serve as a virtual intermediate state with large transition moment provided $E_g^{\Gamma}-E_g^{X}\approx 0$. The alloy disorder potential mixes k states from near the zone center with those near the zone edge. Such random mixing by the short-range potential causes the no-phonon absorption transitions for photon energies at E_g^X.[18] These precedents support our argument that the intermediate Raman-state electron does indeed scatter to the X valley.

Near crossover, kinematical considerations give a much shorter inelastic mean free path in the X valleys than in the Γ valley. This inequality persists even considerably above crossover.

We assume, then, that the inelastic mean free path is so short that different values of x with their different local values of band gap and phonon energies are sampled in our experiments. In this picture the most probable phonon frequency seen via the forbidden Fröhlich process is determined by a weighted average over composition[9]

$$\langle \omega_0'(E_L)\rangle = \frac{\int_0^1 dx\, \omega_0'(x) I(x,E_L)}{\int_0^1 dx\, I(x,E_L)} , \quad (1)$$

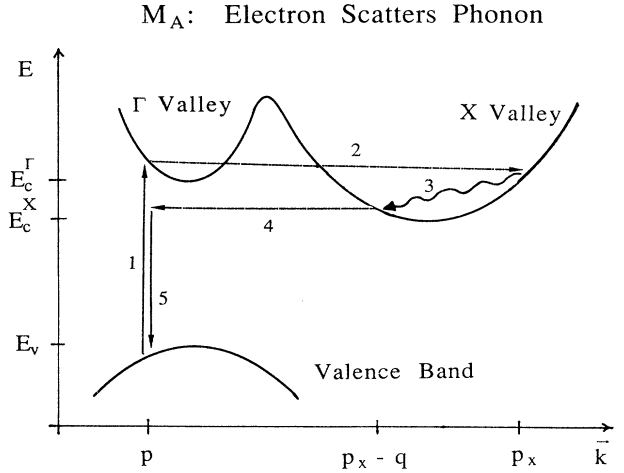

FIG. 14. Resonant Raman process M_A wherein the electron-phonon complex exhibits local alloy properties. The electron-hole pair is created at the direct valley in (1), the electron is scattered by the alloy potential disorder to the indirect valley in (2), a phonon is emitted in (3), the electron returns to the direct valley in (4), and recombination leads to photon emission (5).

where x is the alloy concentration, $\omega_0'(x)$ is the concentration-dependent phonon frequency, E_L is the incident laser energy, and $I(x,E_L)$ is the Raman-scattering efficiency. $I(x,E_L)$ is proportional to the square of the Raman tensor and describes the relative LO-phonon-scattering probability at concentration x for laser energy E_L.

B. Second-order calculation via the X valley

We calculate using perturbation theory in which the electron-hole pair is created and eventually annihilated

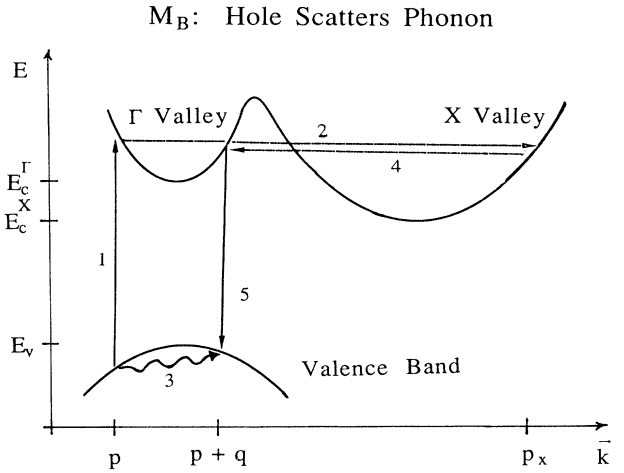

FIG. 15. Complement resonant Raman process M_B to that shown in Fig. 14. In this case the hole emits the phonon.

by photon absorption and emission. The electron scatters twice off the random potential, and either the electron or hole emits a LO phonon via the Fröhlich interaction. There are six terms in the Raman susceptibility from this process. We calculate the two most resonant and most relevant terms, M_A describing electron-phonon scattering in the indirect valley and M_B describing hole-phonon scattering at the direct gap. Figures 14 and 15 illustrate the M_A and M_B processes. We ignore the four other time-permuted orderings. These describe two cases of phonon emission in the direct valley by a lifetime broadened electronic state and the two complementary processes for phonon emission by a lifetime-broadened hole state. The negative experimental results for the shift of the phonon frequency with photon energy at the split-off gap of the direct alloy justify our neglect of their contribution.

M_A represents a five-step process: (1) creation of the direct-gap electron-hole pair, (2) electron scattering to the X valley, (3) X-valley electron-phonon emission, (4) electron scattering back to the Γ valley, and (5) direct-gap electron-hole pair recombination. The calculation of M_A is based on Martin's model,[19] under the following assumptions: zero photon momentum, alloy disorder scatters only the electron with matrix element $V(\mathbf{p})$, and the Fröhlich interaction scatters either the electron, with matrix element c_F/q, or the hole, with matrix element $-c_F/q$. We disregard excitonic effects in this calculation; this matter will be addressed below in the discussion section. The expression for M_A is given by

$$M_A=\frac{\Omega}{V_s}\sum_{\mathbf{p}}\sum_{\mathbf{p}_X}\frac{E_{cv}V(\mathbf{p}_X-\mathbf{p})(\Omega^{-1/2}c_F/q)V(-\mathbf{p}_X+\mathbf{q}+\mathbf{p})}{(E_g^\Gamma+p^2/2\mu_\Gamma-E_L)(E_g^X+p_X^2/2m_X+p^2/2m_h-E_L)}\times\left[\left[E_g^X+\frac{(\mathbf{p}_X-\mathbf{q})^2}{2m_X}+\frac{p^2}{2m_h}+\hbar\omega_0-E_L\right]\left[E_g^\Gamma+\frac{p^2}{2\mu_\Gamma}+\hbar\omega_0-E_L\right]\right]^{-1}, \tag{2}$$

where V_S is the sample scattering volume, Ω is the unit cell volume, E_{cv} is a product of two interband optical matrix elements, $\mathbf{p}$ describes the crystal momentum of the electron in the direct (Γ) valley, $\mathbf{p}_X$ is the crystal momentum in the indirect valley (X), $\mathbf{q}$ is the phonon momentum ($\hbar$ is suppressed for notational simplicity), c_F is the Fröhlich constant, $E_g^\Gamma=E_g^\Gamma(x)$ the concentration-dependent direct energy gap, $E_g^X=E_g^X(x)$ the concentration-dependent indirect energy gap, μ_Γ is the reduced mass at the direct gap, m_h is the hole effective mass, m_X is the indirect-valley electron effective mass, and $\hbar\omega_0$ is the phonon energy. M_B is a nearly identical process to M_A except that the hole scatters the phonon. It is given by

$$M_B=-\frac{\Omega}{V_s}\sum_{\mathbf{p}}\sum_{\mathbf{p}_X}\frac{E_{cv}V(\mathbf{p}_X-\mathbf{p})(\Omega^{-1/2}c_F/q)V(-\mathbf{p}_X+\mathbf{q}+\mathbf{p})}{(E_g^\Gamma+p^2/2\mu_\Gamma-E_L)(E_g^X+p_X^2/2m_X+p^2/2m_h-E_L)}\times\left[\left[E_g^X+\frac{(\mathbf{p}+\mathbf{q})^2}{2m_h}+\frac{p_X^2}{2m_X}+\hbar\omega_0-E_L\right]\left[E_g^\Gamma+\frac{p^2}{2\mu_\Gamma}+\hbar\omega_0-E_L\right]\right]^{-1}. \tag{3}$$

To obtain the Raman tensor, we set $1/m_h$ equal to zero and collect M_A and M_B over a common denominator, yielding

$$M_{A+B}(\mathbf{q})=\frac{\Omega}{V_s}\sum_{\mathbf{p},\mathbf{p}_X}\frac{E_{cv}V(\mathbf{p}_X-\mathbf{p})(\Omega^{-1/2}c_F/q)V(-\mathbf{p}_X+\mathbf{q}+\mathbf{p})}{[p^2-p_{\Gamma L}^2(x)+i\gamma_\Gamma][p_X^2-p_{XL}^2(x)+i\gamma_x][p^2-p_{\Gamma S}^2(x)+i\gamma_\Gamma]}\times(2m_\Gamma)^2(2m_X)^2\left[\frac{1}{[(\mathbf{p}_X-\mathbf{q})^2-p_{XS}^2(x)+i\gamma_X]}-\frac{1}{[p_X^2-p_{XS}^2(x)+i\gamma_X]}\right]. \tag{4}$$

Damping has been introduced explicitly via $E_g^\beta \Longrightarrow E_g^\beta+i\gamma'_\beta$, and the following quantities have been defined and appear in Eq. (4):

$$\gamma_\beta\equiv 2m_\beta\gamma'_\beta, \tag{5}$$

$$p_{\Gamma L}^2(x)=p_{\Gamma L}^2(x,E_L)\equiv 2m_\Gamma[E_L-E_g^\Gamma(x)], \tag{6}$$

$$p_{XL}^2(x)=p_{XL}^2(x,E_L)\equiv 2m_X[E_L-E_g^X(x)], \tag{7}$$

$$p_{\Gamma S}^2(x)=p_{\Gamma S}^2(x,E_L)\equiv 2m_\Gamma[E_L-E_g^\Gamma(x)-\hbar\omega_0], \tag{8}$$

and

$$p_{XS}^2(x)=p_{XS}^2(x,E_L)\equiv 2m_X[E_L-E_g^X(x)-\hbar\omega_0]. \tag{9}$$

The weakly energy-dependent electronic widths γ'_β are assumed to be independent of the electronic momentum. The data of Trallero-Giner, Gavrilenko, and Cardona[20] have provided the direct-gap broadening values.

The Raman-scattering efficiency for the frequency shift ω_0 is

$$\frac{dR}{d\omega_0}=\sum_q |M_{A+B}(q)|^2\delta(\omega_0(q)-\omega_0) , \tag{10}$$

where $\omega_0(q)$ represents the dispersion of the LO phonon. However, the random-alloy potential necessitates proper manipulation of the Raman tensor M_{A+B}. Since it is the fluctuations in V that generate the scattering, we must take a configuration average

$$I(q)=\langle M_{A+B}(\mathbf{q})M^*_{A+B}(\mathbf{q})\rangle . \tag{11}$$

$M_{A+B}(q)$ is written as a product of the random potentials and a catchall function $f(\mathbf{q},\mathbf{p},\mathbf{p}_X)$ to produce

$$I(q)=\left\langle 2\sum_{\mathbf{p},\mathbf{p}'}\sum_{\mathbf{p}_X,\mathbf{p}'_X} f(\mathbf{q},\mathbf{p},\mathbf{p}_X)V(\mathbf{p}_X-\mathbf{p})V(-\mathbf{p}_X+\mathbf{p}+\mathbf{q})f^*(\mathbf{q},\mathbf{p}',\mathbf{p}'_X)V^*(\mathbf{p}'_X-\mathbf{p}')V^*(-\mathbf{p}'_X+\mathbf{p}'+\mathbf{q})\right\rangle . \tag{12}$$

To compute the matrix element $V(\mathbf{p})$ for the electron scattering from $\mathbf{k}$ to $\mathbf{k}+\mathbf{p}$, the electronic wave functions are taken to be plane-wave states, giving

$$V(p)=\langle k+p|V(r)|k\rangle=\frac{1}{V_s}\int d^3r\sum_{\mathbf{R}}u(\mathbf{r}-\mathbf{R})V_{\mathbf{R}}e^{-i\mathbf{q}\cdot\mathbf{r}} , \tag{13}$$

where the sum is over the set $\mathbf{R}$ of Bravais lattice points. $V_{\mathbf{R}}$ is a discreet random variable with zero mean, and we make the simple assumption that $u(\mathbf{r})=1$ if $\mathbf{r}$ is the unit cell at the origin and $u(\mathbf{r})=0$ otherwise. The real-space integration of u gives approximately $a_0^3/4$, the volume of a unit cell. Thus $V(\mathbf{p})$ becomes

$$V(\mathbf{p})=\frac{1}{N}\sum_{\mathbf{R}}V_{\mathbf{R}}e^{-i\mathbf{p}\cdot\mathbf{R}} , \tag{14}$$

where N is the total number of unit cells, that is, $Na_0^3/4=V_s$. Assuming uncorrelated occupancy of the two types of atoms (Ga or Al) on different sites, we use

$$\langle V(\mathbf{k})V^*(\mathbf{k}')\rangle=\frac{\delta_{\mathbf{k},\mathbf{k}'}}{N}\langle V_0^2\rangle , \tag{15}$$

where $V_0\equiv V_{\mathbf{R}=0}$ and where $\langle V_0^2\rangle$ is the mean square of the potential fluctuation at a single site. Applying this expression to Eq. (12), we obtain, for $q\neq 0$,

$$\langle V(\mathbf{p}_X-\mathbf{p})V(-\mathbf{p}_X+\mathbf{p}+\mathbf{q})V^*(\mathbf{p}'_X-\mathbf{p}')V^*(-\mathbf{p}'_X+\mathbf{p}'+\mathbf{q})\rangle=\frac{\langle V_0^2\rangle^2}{N^2}(\delta_{\mathbf{p}'_X,\mathbf{p}_X-\mathbf{p}+\mathbf{p}'}+\delta_{\mathbf{p}'_X,\mathbf{q}+\mathbf{p}'+\mathbf{p}-\mathbf{p}_X}) . \tag{16}$$

By neglecting $\mathbf{p}$ and $\mathbf{p}'$ relative to $\mathbf{p}_X$ in evaluating the f functions, we find that the Raman intensity $I(x,E_L)$ reduces to an integral over $\mathbf{q}$ of

$$I(q)=\sum_{\mathbf{p},\mathbf{p}'}\sum_{\mathbf{p}_X}[f(\mathbf{q},\mathbf{p},\mathbf{p}_X)f^*(\mathbf{q},\mathbf{p}',\mathbf{p}_X)+f(\mathbf{q},\mathbf{p},\mathbf{p}_X)f^*(\mathbf{q},\mathbf{p}',\mathbf{q}-\mathbf{p}_X)]\frac{\langle V_0^2\rangle^2}{N^2} . \tag{17}$$

The sums are converted into integral expressions using

$$\sum_{\mathbf{p}}F(p)=\frac{V_s}{h^3}\int d\mathbf{p}\,F(p) , \tag{18}$$

and the squared Raman matrix element is

$$I(q)=(2m_\Gamma)^4(2m_X)^4\frac{E_{cv}^2}{2}\left[\Omega^{-1/2}\frac{c_F}{q}\right]^2\frac{\langle V_0^2\rangle^2}{N}\frac{\Omega^3}{h^9}\left|\int d^3p\frac{1}{(p^2-p_{\Gamma L}^2+i\gamma_\Gamma)(p^2-p_{\Gamma S}^2+i\gamma_\Gamma)}\right|^2$$
$$\times\int d\mathbf{p}_X\left|\frac{1}{[(\mathbf{p}_X-\mathbf{q})^2-p_{XL}^2+i\gamma_X]}-\frac{1}{(p_X^2-p_{XL}^2+i\gamma_X)}\right|^2\left|\frac{1}{[(\mathbf{p}_X-\mathbf{q})^2-p_{XS}^2+i\gamma_X]}-\frac{1}{(p_X^2-p_{XS}^2+i\gamma_X)}\right|^2 . \tag{19}$$

We now describe the procedure for averaging over x. [Recall that $p_{\Gamma L}$, $p_{\Gamma S}$, p_{XL}, and p_{XS} depend on x via Eqs. (6)–(9).] The total Raman efficiency is proportional to the integral over $\mathbf{q}$ of $I(q)=I(q,x,E_L)$, multiplied by a weighting factor to describe the relative probability of finding composition x if the mean composition is x_0. This we assume to be given by a Gaussian. Thus

$$I(x,E_L)=\int dq\, 4\pi q^2 I(q,E_g^{\Gamma},E_L)\exp-\left[\frac{(x-x_0)^2}{\sigma_X^2}\right] . \tag{20}$$

The variance σ_x^2 of compositional fluctuations is given by[21]

$$\sigma_X^2=\frac{x_0(1-x_0)}{N_c} , \tag{21}$$

where x_0 is the mean concentration and N_c is the number of unit cells within the effective electron-phonon interaction volume. We assume that this volume Λ^3 is equal to the cube of the inelastic mean free path Λ of the X-valley electron. We thus express Λ as

$$\Lambda=p_X/(m_X\tau_{\rm in}) , \tag{22}$$

where $\tau_{\rm in}$ is the inelastic lifetime. We further assume that for the electron in the X valley the relevant value of p_X in Eq. (22) is not the (virtual) integration variable in Eq. (19), but rather is given by the following expression obtained by treating the intermediate state as real and obeying energy conservation:

$$p_X=\sqrt{2m_X[E_g^{\Gamma}(x_0)-E_g^X(x_0)]} . \tag{23}$$

We therefore obtain

$$\sigma_X^2=x_0(1-x_0)\frac{a_0^3}{4}\Big/\left[\frac{\{2m_X[E_g^{\Gamma}(x_0)-E_g^X(x_0)]\}^{1/2}}{m_X}\tau_{\rm in}\right]^3 . \tag{24}$$

The inelastic lifetime in Eq. (24) is related to the inelastic electronic broadening parameter in the X valley via the general relationship $\gamma'=\hbar/2\tau$, and our fitting parameter becomes $\gamma'_{X\rm in}$. The total broadening parameter γ'_X appearing in Eq. (5) [and hence in Eq. (4)] obeys $\gamma'_X=\gamma'_{X\rm in}+\gamma'_{X\rm el}$. The elastic scattering rate $\gamma'_{\rm el}$ is assumed to be dominated by scattering to the X valley and therefore to be the same in both X and Γ valleys. Numerically it should be somewhat smaller than $\gamma'_{X\rm in}$. In the model γ'_{Γ} is the direct-gap broadening. For the Γ valley we assume that $\gamma'_{\Gamma\rm in}\ll\gamma'_{\rm el}$; i.e., we assume that the electron scatters elastically from Γ to X before it has time to emit a LO phonon in Γ. Thus we shall use $\gamma'_{\Gamma}\approx\gamma'_{\rm el}$ in Eqs. (4) and (5).

We return to the evaluation of Eq. (19) and the Γ-valley integration over momentum I_p. Application of residue theory yields

$$|I_p|^2=\frac{4\pi^4}{w_{\Gamma}^2}\left\{(p_{\Gamma L}^4+\gamma_{\Gamma}^2)^{1/2}+(p_{\Gamma S}^4+\gamma_{\Gamma}^2)^{1/2}-2(p_{\Gamma L}^4+\gamma_{\Gamma}^2)^{1/4}(p_{\Gamma S}^4+\gamma_{\Gamma}^2)^{1/4}\cos\frac{1}{2}\left[\tan^{-1}\left[\frac{\gamma_{\Gamma}}{p_{\Gamma L}^2}\right]-\tan^{-1}\left[\frac{\gamma_{\Gamma}}{p_{\Gamma S}^2}\right]\right]\right\} . \tag{25}$$

The X-valley integration is outlined in the Appendix. We define the following quantities to discuss those results:

$$a\equiv(p_{XL}^2+\gamma_X^2)^{1/4}\cos\theta_{XL} , \tag{26}$$

$$b\equiv(p_{XL}^2+\gamma_X^2)^{1/4}\sin\theta_{XL} , \tag{27}$$

$$c\equiv(p_{XS}^2+\gamma_X^2)^{1/4}\cos\theta_{XS} , \tag{28}$$

$$d\equiv(p_{XS}^2+\gamma_X^2)^{1/4}\sin\theta_{XS} , \tag{29}$$

$$\theta_{XS}\equiv\frac{1}{2}\tan^{-1}\left[\frac{\gamma_X}{p_{XS}^2}\right] , \tag{30}$$

$$\theta_{XL}\equiv\frac{1}{2}\tan^{-1}\left[\frac{\gamma_X}{p_{XL}^2}\right] , \tag{31}$$

$$w_X\equiv 2m_X\hbar\omega_0 , \tag{32}$$

$$\Sigma_b=\tan^{-1}\left[\frac{2qb}{q^2+w_X-2qa}\right]+\tan^{-1}\left[\frac{2qb}{q^2+w_X+2qa}\right] , \tag{33}$$

$$\Sigma_d=\tan^{-1}\left[\frac{2qd}{q^2-w_X-2qc}\right]+\tan^{-1}\left[\frac{2qd}{q^2-w_X+2qc}\right] , \tag{34}$$

$$\Delta_{bw}=\tan^{-1}\left[\frac{2\gamma_X+2qb}{q^2+w_X+2qa}\right]+\tan^{-1}\left[\frac{2\gamma_X-2qb}{q^2+w_X-2qa}\right], \tag{35}$$

$$\Delta_{dw}=\tan^{-1}\left[\frac{2\gamma_X+2qd}{q^2-w_X+2qc}\right]+\tan^{-1}\left[\frac{2\gamma_X-2qd}{q^2-w_X-2qc}\right], \tag{36}$$

$$\Delta_{d}=\tan^{-1}\left[\frac{2\gamma_X-2qd}{q^2-2qc}\right]-\tan^{-1}\left[\frac{2\gamma_X+2qd}{q^2+2qc}\right], \tag{37}$$

and

$$\Delta_{b}=\tan^{-1}\left[\frac{2\gamma_X-2qb}{q^2-2qa}\right]-\tan^{-1}\left[\frac{2\gamma_X+2qb}{q^2+2qa}\right]. \tag{38}$$

The result of the X-valley integration I_{p_X} times the valley multiplicity is

$$\begin{aligned}3I_{p_X}=&\frac{6\pi^2w_X^2}{q4\gamma_X^2(w_X^2+4\gamma_X^2)}(\Sigma_b+\Sigma_d)-\frac{6\pi^2(4\gamma_X^2-w_X^2)}{q4\gamma_X^2w_X^2}(\Delta_{bw}+\Delta_{dw})\\&-\frac{6\pi^24\gamma_X^2}{qw_X^2(w_X^2+4\gamma_X^2)}(\Delta_b+\Delta_d)+\frac{24\pi^2}{w_X^2+4\gamma_X^2}\left[\frac{a+c}{2\gamma_X}+\frac{b-d}{w_X}\right]\\&+\frac{3\pi^2}{qw_X\gamma_X}\ln\left[\frac{(q^2-w_X+2qc)^2+(2\gamma_X+2qd)^2}{(q^2-w_X-2qc)^2+(2\gamma_X-2qd)^2}\right]\left[\frac{(q^2+w_X-2qa)^2+(2\gamma_X-2qb)^2}{(q^2+w_X+2qa)^2+(2\gamma_X+2qb)^2}\right].\end{aligned} \tag{39}$$

C. First-order calculation via Γ

To compare to this above-outlined process that was of second order in the random potential V, we now calculate a Raman amplitude that is first order in V for electron scattering in the Γ valley. This is the dominant process in direct III-V alloys. Since the Raman efficiency is proportional to q^2, this disorder-assisted process prevails over the intrinsic one because relaxed momentum restrictions allow larger wave vectors. By analogy, scattering to the X valley enables even larger wave vectors. Two of the four perturbative terms are shown in Fig. 16 and described below. This scattering calculation is based on our earlier model, although it is one order lower in the random potential. M_1 describes a four-step process: (1) creation of the electron-hole pair, (2) electron scattering in the Γ valley by $V(-\mathbf{q})$ the random-valley potential, (3) electron-phonon emission, and (4) direct-gap electron-hole pair recombination:

$$M_1=\frac{\Omega}{V_s}\sum_{\mathbf{p}}\frac{E_{cv}V(-\mathbf{q})(\Omega^{-1/2}c_F/q)}{(E_g^\Gamma+p^2/2\mu_\Gamma-E_L)\left[E_g^\Gamma+(\mathbf{p}+\mathbf{q})^2/2m_\Gamma+\frac{p^2}{2m_h}-E_L\right](E_g^\Gamma+p^2/2\mu_\Gamma+\hbar\omega_0-E_L)}. \tag{40}$$

M_2 is identical to M_1 except that steps (2) and (3) are interchanged:

$$M_1=\frac{\Omega}{V_s}\sum_{\mathbf{p}}\frac{E_{cv}V(-\mathbf{q})(\Omega^{-1/2}c_F/q)}{[E_g^\Gamma+(\mathbf{p}+\mathbf{q})^2/2\mu_\Gamma+\hbar\omega_0-E_L][E_g^\Gamma+(\mathbf{p}+\mathbf{q})^2/2m_h+p^2/2m_\Gamma+\hbar\omega_0-E_L][E_g^\Gamma+(\mathbf{p}+\mathbf{q})^2/2\mu_\Gamma-E_L]}. \tag{41}$$

M_3 consists of (1) electron-hole pair creation at the direct gap, (2) electron scattering in the Γ valley by $V(-\mathbf{q})$, (3) hole-phonon emission, and (4) direct-gap electron-hole pair recombination:

$$M_3=\frac{\Omega}{V_s}\sum_{\mathbf{p}}\frac{-E_{cv}V(-\mathbf{q})(\Omega^{-1/2}c_F/q)}{(E_g^\Gamma+p^2/2\mu_\Gamma-E_L)[E_g^\Gamma+(\mathbf{p}+\mathbf{q})^2/2m_\Gamma+p^2/2m_h-E_L][E_g^\Gamma+(\mathbf{p}+\mathbf{q})^2/2\mu_\Gamma+\hbar\omega_0-E_L]}. \tag{42}$$

M_4 is equal to M_3 with steps (2) and (3) reversed:

$$M_3=\frac{\Omega}{V_s}\sum_{\mathbf{p}}\frac{-E_{cv}V(-\mathbf{q})(\Omega^{-1/2}c_F/q)}{[E_g^\Gamma+(\mathbf{p}+\mathbf{q})^2/2\mu_\Gamma+\hbar\omega_0-E_L][E_g^\Gamma+(\mathbf{p}+\mathbf{q})^2/2m_h+p^2/2m_\Gamma+\hbar\omega_0-E_L](E_g^\Gamma+p^2/2\mu_\Gamma-E_L)}. \tag{43}$$

We sum these four expressions, extract the leading term in $1/m_h$, then set that quantity to zero in the other factors, and introduce broadening via γ_Γ to produce

$$M_{1+2+3+4}=G(q)\sum_p \left[\frac{(q^2+2\mathbf{p}\cdot\mathbf{q})^2}{[p^2-p_{\Gamma S}^2(x)+i\gamma_\Gamma]^2} \left[\frac{1}{[(\mathbf{p}+\mathbf{q})^2-p_{\Gamma S}^2(x)+i\gamma_\Gamma]^2} - \frac{1}{[(\mathbf{p}+\mathbf{q})^2-p_{\Gamma L}^2(x)+i\gamma_\Gamma]^2} \right] + \frac{(q^2+2\mathbf{p}\cdot\mathbf{q})^2}{[p^2-p_{\Gamma L}^2(x)+i\gamma_\Gamma]^2} \left[\frac{1}{[(\mathbf{p}+\mathbf{q})^2-p_{\Gamma L}^2(x)+i\gamma_\Gamma]^2} - \frac{1}{[(\mathbf{p}+\mathbf{q})^2-p_{\Gamma S}^2(x)+i\gamma_\Gamma]^2} \right] \right], \quad (44)$$

where $G(q)$ is designated by

$$G(q)=\frac{\Omega}{V_s}E_{cv}V(-\mathbf{q})\left[\Omega^{-1/2}\frac{c_F}{q}\right]\frac{(2m_\Gamma)^4}{2m_h w_\Gamma^2} . \quad (45)$$

The sum over p is converted into an integral which is evaluated by residue theory. We take a configurational average of $|M|^2$ to obtain the Raman intensity:

$$I(q)=\langle M_{1+2+3+4}(\mathbf{q})M^*_{1+2+3+4}(\mathbf{q})\rangle . \quad (46)$$

The final expression for the Raman susceptibility in the Γ valley is

$$I(q)=E_{cv}^2\left[\Omega^{-1/2}\frac{c_F}{q}\right]^2\frac{\langle V_0^2\rangle}{N}\frac{\Omega^2}{h^6}\frac{64\pi^4 m_\Gamma^8}{m_h^2} \times\left|\frac{q^2\{q^2-[(p_{\Gamma L}^2-i\gamma_\Gamma)^{1/2}-(p_{\Gamma S}^2-i\gamma_\Gamma)^{1/2}]^2\}}{(p_{\Gamma L}^2-i\gamma_L)^{1/2}(p_{\Gamma S}^2-i\gamma_\Gamma)^{1/2}[(p_{\Gamma L}^2-i\gamma_\Gamma)^{1/2}+(p_{\Gamma S}^2-i\gamma_\Gamma)^{1/2}][q^4-2q^2(p_{\Gamma L}^2+p_{\Gamma S}^2-2i\gamma_\Gamma)+w_\Gamma^2]}\right|^2 . \quad (47)$$

The calculated Raman cross sections for the first- and second-order disorder-potential-mediated scattering have the expected leading-order q^2 functional dependence. This is explicitly evident in the first-order calculation of Eq. (47). The symmetry of the second-order result [Eq. (39)] dictates that all odd-powered terms in q must be zero, and the q^{-2} and q^0 terms exactly cancel.

D. Evaluation and discussion of theoretical results

1. *Second-order impurity scattering via X valleys versus first-order scattering in the Γ valley*

The complicated q dependence of the analytic Raman expressions motivates a numerical comparison over a discrete range of laser energies and values of q appropriate to the resonance. Prior to the integration over Al concentration, we calculate the ratio of the q integrands, $I_{\text{second order}}/I_{\text{first order}}$. We evaluated this quantity for laser energies equal to E_g^Γ plus $n\hbar\omega_0$, where $n=0$, 0.5, 1.0, and 1.5 and for momentum values $\hbar q$ from 0 to $\sqrt{2m_X\omega_0}$. The density-of-states effective mass used was given by $M_X=(m_{Xt}^2 m_{Xl})^{1/3}$, geometrical mean of longitudinal and transverse X-valley masses. Table III lists these values and their x dependence for this calculation. Figure 17 shows typical results for $Al_{0.5}Ga_{0.5}As$ and $Al_{0.7}Ga_{0.3}As$ evaluated at the peak of the outgoing resonance. Note that the second-order process is stronger

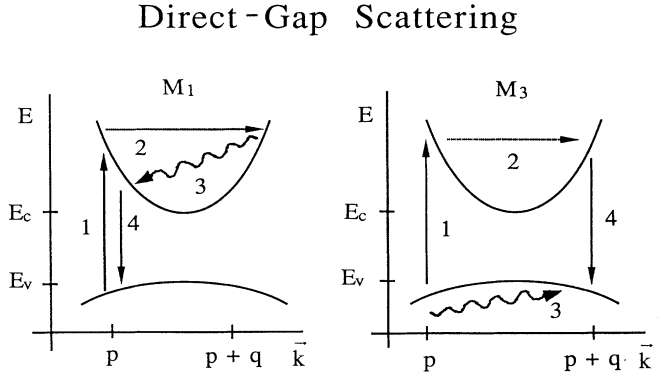

FIG. 16. Two perturbative terms of first order in the random potential V contributing to the Raman scattering. M_1 shows the creation of an electron-hole pair in (1), the electron is scattered by the alloy potential in (2), a phonon is emitted in (3), and recombination occurs in (4). M_3 is equivalent to M_1 save the phonon is emitted by the hole.

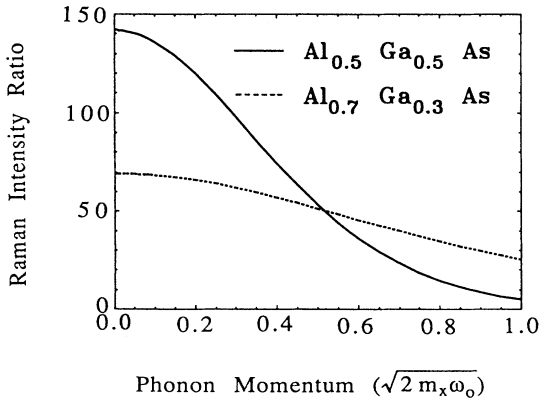

FIG. 17. Ratio for the calculation of the intensity of the second-order disorder-potential scattering to the first-order random-alloy scattering vs phonon wave vector. The solid line corresponds to $Al_{0.5}Ga_{0.5}As$, the dotted line is for $Al_{0.7}Ga_{0.3}As$, and pertinent parameters are listed in Table III.

than the first-order process by a factor of about 10^2 for small q. Note that the q range in Fig. 17 is roughly double the maximum value of q for the direct gap, which is given by $\sqrt{2m_\Gamma\omega_0}$; the q_{cutoff} for the indirect case is at least $\sqrt{2m_{Xl}\omega_0}$. We varied the parameters $\gamma'_{X\text{in}}$, x_0, and E_L and produced similar results. The intensity ratio ranged from 10^1 to 10^3. Uncertainty in the crossover concentrations is compensated for by examining several fixed values for $E_g^\Gamma - E_g^X$. Figure 17 has $E_g^\Gamma - E_g^X$ equal to $2\hbar\omega_0$ for $Al_{0.5}Ga_{0.5}As$ and $8\hbar\omega_0$ for $Al_{0.7}Ga_{0.3}As$. As expected, the shift effect weakens as crossover is approached.

2. Calculation of the dependence of phonon frequency on laser photon energy

The calculation of $\langle \omega'_0(E_L) \rangle$ [Eq. (1)] involves numerical integration over q and x for appropriate laser energies in order to generate the resonance profile and shift behavior. We show a sample calculated resonance profile and shift result for the dipole-forbidden LO_2 mode in Fig. 18. Two shortcomings of our model are immediately evident upon attempting to match Fig. 18 with the experimental results. The peak energy of the calculated resonance occurs near $E_g^\Gamma + \frac{1}{2}h\omega_0$, and the resonance profile full width at half maximum is very wide, in fact too wide by a factor of 2 for the samples near crossover. These difficulties are rooted in the use of a free-electron–hole pair model. As demonstrated by Trallero-Giner, Cantarero, and Cardona,[22] excitons play a decisive role in the one-phonon Fröhlich-mediated Raman process. The discrete-to-continuous transitions, that is, phonon processes connecting a discrete exciton with an exciton in the continuum, are the most important transitions. They provide the asymmetry between the ingoing and outgoing resonances; the large excitonic oscillator strength sharpens spectral features. However, an excitonic calculation that would include disorder in a meaningful way exceeds the scope of this paper and merits its own full theoretical investigation. Thus a detailed comparison between theory and experiment on our part is unwarranted. Instead, we emphasize that we have demonstrated theoretically that the second-order scattering process via the X valley is dominant over the lower-order Γ-valley case.

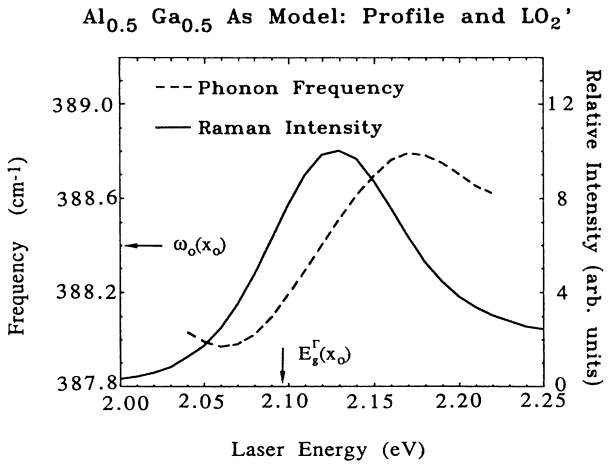

FIG. 18. Results of the model calculation for $Al_{0.5}Ga_{0.5}As$ with the resonance profile indicated by the solid line and the phonon frequency for $LO_{2'}$ given by the dotted line. The arrows indicate the direct gap at 2.096 eV and the mean frequency at 388.4 cm^{-1}.

Recent work of Trallero-Giner *et al.*[23] examined the dipole-forbidden resonance profiles of indirect $Al_{1-x}Ga_xAs$ alloys. They accounted for the disorder-induced dipole-forbidden LO-phonon scattering by multiplying the intrinsic Fröhlich polarizability by an adjustable parameter. They noted discrepancies in their model. Although their treatment includes the contributions from both discrete and continuous excitonic states, it does not account for the shift which we have extensively discussed here.

Although our model is unable to provide a quantitative fit, it does account for the functional dependence of the resonance on the lifetimes. The one arbitrary fitting parameter in the model is the X-valley inelastic lifetime. We observe both experimentally and theoretically that the resonance profiles broaden and the shifts weaken as γ'_{el}, the elastic-scattering rate, increases. The sharp change in slope between the $Al_{0.41}Ga_{0.59}As$ and $Al_{0.42}Ga_{0.58}As$ samples may be caused by a large difference in the elastic scattering; we observe much less luminescent intensity in $Al_{0.42}Ga_{0.58}As$ than in $Al_{0.41}Ga_{0.59}As$. Of course, this change might also be attributed to different magnitudes of compositional fluctuations. Enhanced effective localization caused by an increasing $\gamma'_{X\text{in}}$, the inelastic broadening parameter, generates larger shift slopes and a broader resonance profile. In the case of the $Al_{0.5}Ga_{0.5}As$ model, application of the uncertainty principle leads to an estimate of the X-valley electronic inelastic lifetime of the order of 10 fs.

We also note the additional complication introduced by the presence of the L valley; this has not been included in this calculation. In fact E_g^L, the indirect gap at the L point, crosses the direct gap just above the crossover of E_g^X and E_g^Γ. In addition, we have ignored $\omega_0(q)$ dispersion, which can produce a unidirectional negative shift in frequency as the dominant value is increased by raising the photon energy farther above the direct gap. This effect would appear most strongly when scattering high in the X valley, i.e., when the sample is strongly indirect and wave vectors of large magnitude are expected to dominate. Examination of the GaAs dispersion curve obtained from neutron data shows detectable shifts for wave vectors about one-quarter of the way out of the Brillouin-zone edge.[24] This might explain the absence of positive $\Delta\omega$'s for the AlAs-like mode in our indirect samples $Al_{0.68}Ga_{0.32}As$ and $Al_{0.77}Ga_{0.23}As$.

V. SUMMARY

We have described the laser-frequency-dependent shift of phonon frequency between the dipole-forbidden and dipole-allowed LO modes in disordered $Al_xGa_{1-x}As$ alloys. It results from elastic scattering of the electron

from the Γ valley to the X valley and back via the random alloy potential. The heavier, more localized, mass allows shorter-wavelength (large wave vector) phonons to be emitted and manifests the more localized nature of this X-valley process. A Raman susceptibility calculation demonstrates that the magnitude of the Γ-X-Γ second-order process is greater than its first-order Γ-Γ counterpart. As the alloy becomes more indirect, elastic-scattering processes broaden the electronic linewidth and weaken both the resonance and this shift effect.

ACKNOWLEDGMENTS

This work was supported by the NSF under Grants Nos. NSF DMR 88-03108 and through the Materials Research Laboratory under Grant Nos. NSF DMR 83-16981 and 89-20538.

APPENDIX

The X-valley momentum integration generates 16 parts from the integrand consisting of a product of the squares of the difference terms $[(p_X-q)^2-p_{Xi}^2]^{-1}-(p_X^2-p_{Xi}^2)^{-1}$. The mechanical details of this type of contour integral are discussed by Martin[19] in his Appendix A. Application of symmetry arguments reduces the necessary number of integrations to five from 16. We define the following quantities to discuss our results:

$$a\equiv(p_{XL}^2+\gamma_X^2)^{1/4}\cos\theta_{XL}\ , \tag{A1}$$

$$b\equiv(p_{XL}^2+\gamma_X^2)^{1/4}\sin\theta_{XL}\ , \tag{A2}$$

$$c\equiv(p_{XS}^2+\gamma_X^2)^{1/4}\cos\theta_{XS}\ , \tag{A3}$$

$$d\equiv(p_{XS}^2+\gamma_X^2)^{1/4}\sin\theta_{XS}\ , \tag{A4}$$

$$\theta_{XS}\equiv\frac{1}{2}\tan^{-1}\left[\frac{\gamma_X}{p_{XS}^2}\right]\ , \tag{A5}$$

$$\theta_{XL}\equiv\frac{1}{2}\tan^{-1}\left[\frac{\gamma_X}{p_{XL}^2}\right]\ , \tag{A6}$$

and

$$w_X\equiv 2m_X\hbar\omega_0\ . \tag{A7}$$

$I(p_X)_1$ is angularly independent and is given by

$$I(p_X)_1=\int\frac{4\pi p_X^2dp_X}{[(p_X^2-p_{XL}^2)^2+\gamma_X^2]}\times\frac{1}{[(p_X^2-p_{XS}^2)^2+\gamma_X^2]}\ . \tag{A8}$$

We factor this into four poles, and evaluation of the residues produces

$$I(p_X)_1=\frac{4\pi^2}{w_X^2+4\gamma_X^2}\left[\frac{(a+c)}{2\gamma_X}+\frac{(b-d)}{w_X}\right]\ . \tag{A9}$$

$I(p_X)_2$ is $I(p_X)_1$ with p_X replaced by $\mathbf{p}_X-\mathbf{q}$. Since the integration limits are $\pm\infty$, the origin is arbitrary and these two integrals are identical. The factoring of $I(p_X)_3$ by partial fractions greatly simplifies the angular and radial integrals:

$$I(p_X)_3=\int\frac{2\pi p_X^2dp_X}{[(p_X^2-p_{XS}^2)^2+\gamma_X^2]}\times\frac{\sin\theta\,d\theta}{\{[(\mathbf{p}_X-\mathbf{q})^2-p_{XL}^2]^2+\gamma_X^2\}}\ . \tag{A10}$$

The result of this integral is

$$I(p_X)_3=\frac{\pi^2}{4q\gamma_X^2}(\Sigma_b+\Sigma_d-\Delta_{bw}-\Delta_{dw})\ , \tag{A11}$$

where

$$\Sigma_b=\tan^{-1}\left[\frac{2qb}{q^2+w_X-2qa}\right]+\tan^{-1}\left[\frac{2qb}{q^2+w_X+2qa}\right]\ , \tag{A12}$$

$$\Sigma_d=\tan^{-1}\left[\frac{2qd}{q^2-w_X-2qc}\right]+\tan^{-1}\left[\frac{2qd}{q^2-w_X+2qc}\right]\ , \tag{A13}$$

$$\Delta_{bw}=\tan^{-1}\left[\frac{2\gamma_X+2qb}{q^2+w_X+2qa}\right]+\tan^{-1}\left[\frac{2\gamma_X-2qb}{q^2+w_X-2qa}\right]\ , \tag{A14}$$

and

$$\Delta_{dw}=\tan^{-1}\left[\frac{2\gamma_X+2qd}{q^2-w_X+2qc}\right]+\tan^{-1}\left[\frac{2\gamma_X-2qd}{q^2-w_X-2qc}\right]\ . \tag{A15}$$

$I(p_X)_4$ transforms to $I(p_X)_3$ by interchanging L and S subscripted momenta. Thus we transform the previous result by changing a to c, b to d, and w_X to negative w_X, which shows that $I(p_X)_4$ equals $I(p_X)_3$. The next integral is $I(p_X)_5$ whose complex conjugate is $I(p_X)_6$:

$$I(p_X)_5=\int\frac{-2\pi p_X^2dp_X}{[(\mathbf{p}_X-\mathbf{q})^2-p_{XL}^2]^2+\gamma_X^2}\frac{\sin\theta\,d\theta}{[(\mathbf{p}_X-\mathbf{q})^2-p_{XS}^2+i\gamma_X](p_X^2-p_{XS}^2-i\gamma_X)}\ . \tag{A16}$$

The sum result of $I(p_X)_5$ and $I(p_X)_6$ is

$$I(p_X)_{5+6}=\frac{\pi^2}{q(w_X^2+4\gamma_X^2)}(\Delta_b+\Delta_d-\Sigma_b-\Sigma_d)+\frac{\pi^2}{2qw_X\gamma_X}\ln\left[\frac{(q^2-w_X+2qc)^2+(2\gamma_X+2qd)^2}{(q^2-w_X-2qc)^2+(2\gamma_X-2qd)^2}\right]\times\left[\frac{(q^2+w_X-2qa)^2+(2\gamma_X-2qb)^2}{(q^2+w_X+2qa)^2+(2\gamma_X+2qb)^2}\right], \tag{A17}$$

where we define

$$\Delta_d=\tan^{-1}\left[\frac{2\gamma_X-2qd}{q^2-2qc}\right]-\tan^{-1}\left[\frac{2\gamma_X+2qd}{q^2+2qc}\right] \tag{A18}$$

and

$$\Delta_b=\tan^{-1}\left[\frac{2\gamma_X-2qb}{q^2-2qa}\right]-\tan^{-1}\left[\frac{2\gamma_X+2qb}{q^2+2qa}\right]. \tag{A19}$$

Interchanging L and S in $I(p_X)_5+I(p_X)_6$ will give $I(p_X)_7+I(p_X)_8$, which is an identical result because of the summary of the terms. The integrals $I(p_X)_9$ to $I(p_X)_{12}$ transform to the integrals $I(p_X)_5$ to $I(p_X)_8$ by replacing $\mathbf{p}_X$ with $\mathbf{p}_X-\mathbf{q}$. Again, because the choice of origin is arbitrary, the sum $I(p_X)_5+I(p_X)_6+I(p_X)_7I(p_X)_8$ is equivalent to $I(p_X)_9+I(p_X)_{10}+I(p_X)_{11}+I(p_X)_{12}$. The next integral is $I(p_X)_{13}$, given by

$$I(p_X)_{13}=\int\frac{2\pi p_X^2dp_X\sin\theta\,d\theta}{[(\mathbf{p}_X-\mathbf{q})^2-p_{XL}^2+i\gamma_X](p_X^2-p_{XL}^2-i\gamma_X)[(\mathbf{p}_X-\mathbf{q})^2-p_{XS}^2-p_{XS}^2-i\gamma_X]}, \tag{A20}$$

and $I(p_X)_{14}$ is its complex conjugate. Proceeding with the factoring and contour integration produces

$$I(p_X)_{13+14}=\frac{2\pi^2}{q(w_X^2+4\gamma_X^2)}(\Sigma_b+\Sigma_d-\Delta_b-\Delta_d). \tag{A21}$$

Finally, we have $I(p_X)_{15}$ shown by

$$I(p_X)_{15}=\int\frac{2\pi p_X^2dp_X\sin\theta\,d\theta}{[(\mathbf{p}_X-\mathbf{q})^2-p_{XL}^2+i\gamma_X](p_X^2-p_{XL}^2-i\gamma_X)[(\mathbf{p}_X-\mathbf{q})^2-p_{XS}^2+i\gamma_X](p_X^2-p_{XS}^2-i\gamma_X)}, \tag{A22}$$

with its complete conjugate equal to $I(p_X)_{16}$. The sum of these two integrals is

$$I(p_X)_{15+16}=\frac{2\pi^2}{qw_X^2}(\Delta_{bw}+\Delta_{dw}-\Delta_b-\Delta_d). \tag{A23}$$

To account for the valley multiplicity, we assume that the X-valley minimum occurs exactly at the zone boundary. This provides an additional factor of 3 times the result of these 16 integrations:

$$\begin{aligned}3I(P_X)=&\frac{6\pi^2w_X^2}{q4\gamma_X^2(w_X^2+4\gamma_X^2)}(\Sigma_b+\Sigma_d)-\frac{6\pi^2(4\gamma_X^2-w_X^2)}{q4\gamma_X^2w_X^2}(\Delta_{bw}+\Delta_{dw})\\&-\frac{6\pi^24\gamma_X^2}{qw_X^2(w_X^2+4\gamma_X^2)}(\Delta_b+\Delta_d)+\frac{24\pi^2}{w_X^2+4\gamma_X^2}\left[\frac{a+c}{2\gamma_X}+\frac{b-d}{w_X}\right]\\&+\frac{3\pi^2}{qw_X\gamma_X}\ln\left[\frac{(q^2-w_X+2qc)^2+(2\gamma_X+2qd)^2}{(q^2-w_X+2qc)^2+(2\gamma_X+2qd)^2}\right]\left[\frac{(q^2+w_X-2qa^2)+(2\gamma_X+2qb)^2}{(q^2+w_X+2qa)^2+(2\gamma_X+2qb)^2}\right].\end{aligned} \tag{A24}$$

---

*Present address: Intel Corporation, MS SC1-03, P.O. Box 58126, Santa Clara, CA 95052-8126.

†Present address: Department of Physics, Colorado College, Colorado Springs, CO 80903.

[1]R. Tsu, H. Kawamura, and L. Esaki, *Proceedings of the 11th International Conference on the Physics of Semiconductors* (Polish Scientific, Warsaw, 1972), p. 1136.

[2]O. K. Kim and W. G. Spitzer, J. Appl. Phys. **50**, 4362 (1979).

[3]B. Jusserand and J. Sapriel, Phys. Rev. B **24**, 7194 (1981).

[4]P. Paranyanthal and F. Pollack, Phys. Rev. Lett. **52**, 1822 (1984).

[5]J. A. Kash, J. M. Hvam, J. C. Tsang, and T. F. Kuech, Phys. Rev. B **38**, 5776 (1988).

[6]J. Shah, A. DiGiovanni, T. Damen, and B. Miller, Phys. Rev. B **7**, 3481 (1973).

[7]R. Beserman, K. P. Jain, M. V. Klein, and H. Morkoç, in *Proceedings of the Second International Conference on Phonon Physics,* edited by J. Kollar, N. Kroo, N. Menyhard, and T.

Siklos (World Scientific, Singapore, 1985), p. 245.
[8]T. C. McGlinn, M. V. Klein, and H. Morkoç, Bull. Am. Phys. Soc. **32**, 801 (1987).
[9]I. Sela, V. V. Gridin, R. Beserman, R. Sarfaty, and D. Fekete, J. Appl. Phys. **63**, 966 (1988).
[10]R. M. Martin, Phys. Rev. B **4**, 3676 (1971).
[11]A. A. Gogolin and E. I. Rashba, Solid State Commun. **19**, 1177 (1976).
[12]J. Menendez, M. Cardona, and L. Vodopyanov, Phys. Rev. B **31**, 3705 (1985).
[13]C. Bosio, J. L. Staehli, M. Guzzi, G. Burri, and R. A. Logan, Phys. Rev. B **38**, 3263 (1988).
[14]S. Adachi, J. Appl. Phys. **58**, R1 (1985), and referencces cited therein.
[15]H. J. Lee, L. Y. Juravel, and J. C. Woolley, Phys. Rev. B **21**, 659 (1980).
[16]M. D. Sturge, E. Cohen, and R. A. Logan, Phys. Rev. B **27**, 2362 (1983).
[17]R. Dingle, R. A. Logan, and R. J. Nelson, Solid State Commun. **29**, 171 (1979).
[18]M. V. Klein, M. D. Sturge, and E. Cohen, Phys. Rev. B **25**, 4331 (1982).
[19]R. M. Martin, Phys. Rev. B **10**, 2620 (1974).
[20]C. Trallero-Giner, V. I. Gavrilenko, and M. Cardona, Phys. Rev. B **40**, 1238 (1989).
[21]E. F. Schubert, E. O. Gobel, Y. Horikashi, K. Ploog, and H. J. Queisser, Phys. Rev. B **30**, 813 (1984).
[22]C. Trallero-Giner, A. Cantarero, and M. Cardona, Phys. Rev. B **40**, 4030 (1989).
[23]C. Trallero-Giner, A. Cantarero, M. Cardona, and V. I. Gavrilenko, Phys. Rev. B **42**, 11 875 (1991).
[24]J. T. Waugh and G. Dolling, Phys. Rev. **132**, 2410 (1963).